Journal of Guidance, Control, and Dynamics
Vol. 33, No. 6, November–December 2010

Constrained Multiple-Revolution Lambert's Problem

Gang Zhang* and Daniele Mortari†
Texas A&M University, College Station, Texas 77843-3141
and
Di Zhou‡
Harbin Institute of Technology, 150001 Harbin, People's Republic of China

DOI: 10.2514/1.49683

A fixed-time, multiple-revolution Lambert's problem is solved under given constraints. For $N_{\max}$ revolutions, there exist $2N_{\max} + 1$ mathematical solutions to Lambert's problem. Unfortunately, not all of these solutions are feasible. Practical solutions require that the perigee radius be greater than a minimum value (to avoid Earth-impacting trajectories) and the apogee radius be lower than a maximum value (to avoid expensive changes in eccentricity). In particular, short-path and long-path solutions require different considerations to discriminate between the unfeasible solutions. A solution procedure for the semimajor-axis range is proposed that takes these two constraints into account. Based on the semimajor-axis range, the solutions with a feasible number of revolutions can be easily selected. The case of zero revolutions is also discussed, as the trajectory may be feasible even if not complying with the bounds. Numerical examples show that the number of feasible solutions greatly decreases when considering the constraints.

I. Introduction

THE two-point boundary-value problem, known as Lambert's problem (or Lambert's theorem), is a fundamental problem of astrodynamics. The problem consists of the determination of a body's orbit (conic section) given a specified time interval t_f between two position vectors $\mathbf{r}_1$ and $\mathbf{r}_2$. Figure 1 shows the geometry of this problem, where F_1 is the primary focus, P_1 is the initial point, P_2 is the final point, and θ is the transfer angle between the two position vectors $\mathbf{r}_1$ and $\mathbf{r}_2$.

Battin [1] discussed Lambert's problem in detail, and the solution was geometrically found by Lagrange [2] (1778) and Gauss [3] (1809). Lambert's theorem [4] describes this problem using the sum of $r_1 + r_2$ rather than r_1 and r_2 separately. Many other methods [5–8] have been devised to solve Lambert's problem. Of particular interest is the method proposed by Avanzini [9], who provided a solving technique using a simple iterative (Newton–Raphson) algorithm in terms of the transverse eccentricity vector component.

The multiple-revolution Lambert's problem was also discussed in [1,8]. Prussing [10] indicated there are $2N_{\max} + 1$ orbit solutions, where $N_{\max}$ is the maximum number of allowed revolutions for specified transfer time. For a two-impulse rendezvous using multiple-revolution Lambert solutions, Prussing [10] obtained the minimum cost solution by calculating all $2N_{\max} + 1$ candidates. Shen and Tsiotras [11] gave a method for determining the optimal solution by calculating and comparing two candidates, at most. Moreover, for the multiple-impulse, multiple-revolution rendezvous problem, a hybrid optimization approach was proposed [12]. In addition, He et al. [13] extended the analysis method proposed by Avanzini [9] to the multiple revolutions case.

Previous work in the literature concerning the multiple-revolution Lambert's problem did not consider any constraints on the transfer. But in practice, the perigee altitude is usually required to be greater than a minimum value $h_{p\min}$ (lower bound, e.g., $h_{p\min} = 350$ km). In addition, the apogee altitude is usually required to be less than an upper bound $h_{a\max}$. Considering these two bounds, the absolute maximum number of solutions is $2N_{\max} + 1$. The classic approach consists of calculating perigee and apogee altitudes for all the $2N_{\max} + 1$ orbits and then rejecting those solutions that do not satisfy the bounds. This paper propose a different, simpler, and more universal method to remove the unwanted solutions.

This paper gives a solution to the multiple-revolution Lambert's problem with bounds. Based on the orbit categories defined by Shen and Tsiotras [11], the characteristics about different orbit types are first analyzed. Then the bound for the range of semimajor axis is solved in detail. Based on the derived range for the semimajor axis, it is easy to get the number of allowed revolutions and the final orbit solutions. When there are zero revolutions, the trajectory may not pass through the perigee or the apogee, so this case is discussed separately. Finally, a numerical example is given showing that the number of solutions greatly decreases when bounds are considered.

II. Multiple-Revolution Lambert's Problem

A. Transfer Orbit Categories

Given two radius vectors $\mathbf{r}_1$ and $\mathbf{r}_2$ (relative to the focus F_1 at the gravitational center of attraction), there are three orbit categories defined by the location of the vacant focus [11].

1) The *minimum-energy orbit* is shown in Fig. 1, in which the vacant focus F_2 lies on the $\overline{P_1P_2}$ line segment. In this case, the semimajor axis of transfer orbit is

$$a_m = \frac{s}{2} \tag{1}$$

where

$$s = \frac{r_1 + r_2 + d}{2}, \qquad d = |\mathbf{r}_1 - \mathbf{r}_2|$$

which is the length of the chord connecting P_1 and P_2.

2) For $a > a_m$, the *short-path orbit* is shown in Fig. 2.

3) For the same value of a, the *long-path orbit* is also shown in Fig. 2.

The vacant focuses in the short- and long-path orbits are F_2 and F_2^*, respectively, which are symmetric about the connecting line

Received 2 March 2010; revision received 26 May 2010; accepted for publication 29 May 2010.

*Research Scholar, Aerospace Engineering, 743A H. R. Bright Building; zhanggang3110@yahoo.cn.

†Associate Professor, Aerospace Engineering, 746C H. R. Bright Building; mortari@tamu.edu. Associate Fellow AIAA.

‡Professor, Department of Control Science and Engineering; zhoud@hit.edu.cn.

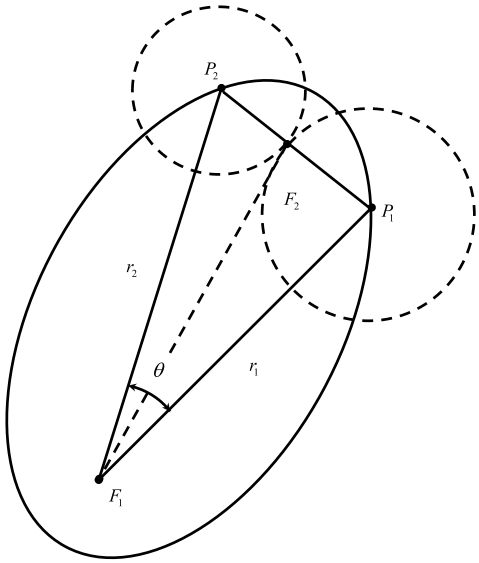

Fig. 1 Minimum-energy orbit.

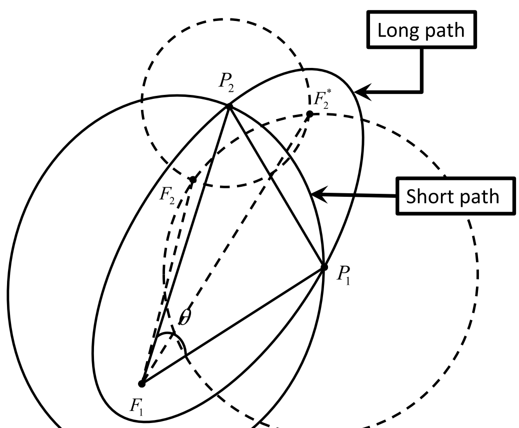

Fig. 2 Short-path and long-path orbits.

$\overline{P_1 P_2}$. As shown in Fig. 2 for a long-path orbit, F_1 and F_2^* lie on opposite sides of the $\overline{P_1 P_2}$ line segment, whereas for a short-path orbit, F_1 and F_2 lie on the same side of the $\overline{P_1 P_2}$ line segment. This paper considers the short- and long-path transfer orbits only, as the minimum-energy-orbit case is an extreme case in which the short- and long-path orbits coincide.

B. Lagrange's Equation of Transfer Time

From Lagrange's formulation of the multiple-revolution Lambert's problem, the relationship between transfer time t_f and semimajor axis a can be expressed as [10]

$$t_f = \sqrt{\frac{a^3}{\mu}}[2\pi N + \alpha - \beta - (\sin\alpha - \sin\beta)] \tag{2}$$

where μ is the gravitational parameter, N is the number of revolutions, and α and β are Lagrange's parameters defined by

$$\cos\alpha = 1 - \frac{s}{a} \quad \text{and} \quad \cos\beta = 1 - \frac{s-d}{a} = \cos\alpha + \frac{d}{a} \tag{3}$$

Let $\cos^{-1}(1 - s/a) = \alpha_0 \in [0, \pi]$ and $\cos^{-1}[1 - (s-d)/a] = \beta_0 \in [0, \pi]$, then from the geometric interpretation of the variables α and β [14], two distinct cases are obtained:

1) If $\theta \le \pi$, then for the short path, $\alpha = \alpha_0$ and $\beta = \beta_0$, while for the long path, $\alpha = 2\pi - \alpha_0$ and $\beta = \beta_0$ [see Eq. (2)].

2) If $\theta \ge \pi$, then for the short path, $\alpha = 2\pi - \alpha_0$ and $\beta = -\beta_0$, while for the long path, $\alpha = \alpha_0$ and $\beta = -\beta_0$ [see Eq. (2)].

Figure 3 provides the transfer times for various values of N and for $r_1 = R_E + 800$ km, $r_2 = 1.2 r_1$, and $\theta = \pi/3$, where $R_E = 6,378.13$ km is the Earth radius. For each N, there are two solution branches: the upper branch (dotted lines) and the lower branch (continuous lines). The upper branch corresponds to long-path transfers for $\theta \le \pi$ and to short-path for $\theta \ge \pi$, while the lower branch is associated with short paths for $\theta \le \pi$ and with long paths for $\theta \ge \pi$.

III. Unbounded Estimation of the Number of Revolutions

This section provides an upper bound of N, that is $N_{\max}$, associated with an assigned value of the transfer time t_f. Differentiating Eq. (2) with respect to a gives

$$\frac{\mathrm{d}t_f}{\mathrm{d}a} = \frac{3}{2}\sqrt{\frac{a}{\mu}}\left[2N\pi + \alpha - \sin\alpha - \frac{4\sin^3(\alpha/2)}{3\cos(\alpha/2)} - \beta + \sin\beta + \frac{4\sin^3(\beta/2)}{3\cos(\beta/2)}\right] \tag{4}$$

Since the number of solutions is $2N_{\max} + 1$, then for $N = 0$, there is no solution associated with $\mathrm{d}t_f/\mathrm{d}a = 0$. This indicates that *the transfer time of the upper branch is monotonically increasing*, while for the lower branch, t_f is monotonically decreasing. If $N \ge 1$, there is a single solution of $\mathrm{d}t_f/\mathrm{d}a = 0$ associated with the lower branch, while no solution for the upper branch, as t_f is monotonically increasing. Hence, for the lower branch, the transfer time first decreases and then monotonically increases.

For an assigned value of N, let $a_{\min N}$ be the solution of $\mathrm{d}t_f/\mathrm{d}a = 0$, and let $t_{\min N}$ be the associated transfer time. From the inequality

$$t_{\min N_{\max}} \le t_f < t_{\min(N_{\max}+1)} \tag{5}$$

the maximum number of revolutions, $N_{\max}$, can be determined. Let $t_{mN_{\max}}$ be the corresponding transfer time for the minimum semimajor axis a_m and $N = N_{\max}$. If

$$t_f < t_{mN_{\max}} \tag{6}$$

then two solutions for the lower branch associated with $N = N_{\max}$ are obtained. For an assigned value of t_f, there are $2N_{\max} + 1$ solutions in total for the multiple-revolution Lambert's problem [10]. The example given in Fig. 3 provides $N_{\max} = 5$; consequently, there are 11 solutions in total for the multiple-revolution Lambert's problem.

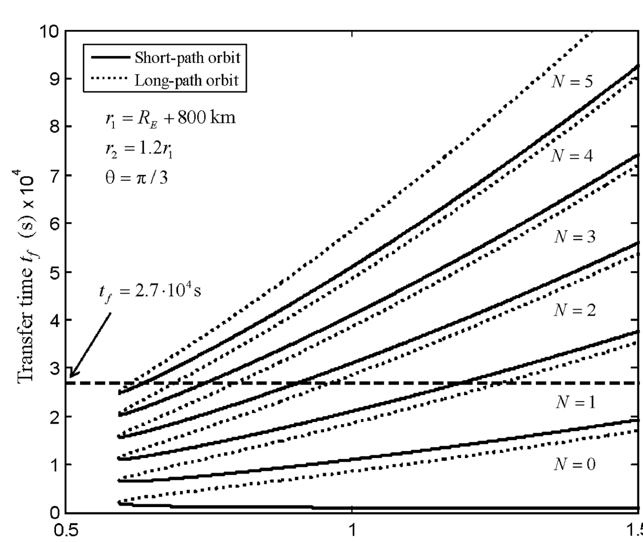

Fig. 3 An example for t_f vs a.

IV. Conditions of Solution Existence

The $2N_{\max} + 1$ solutions are mathematical solutions, as no bound has been enforced on the problem. Feasible solutions require that the perigee altitude be greater than a minimum value $h_{p\min}$ (atmosphere altitude) and an upper bound for the apogee altitude, $h_{a\max}$, to bound the orbit eccentricity, or an upper bound of the semimajor axis, to bound the energy.

Perigee and apogee radii are

$$R_p = R_E + h_{p\min} \quad \text{and} \quad R_a = R_E + h_{a\max} \tag{7}$$

With no loss of generality, consider $r_2 \geq r_1$. Two extreme cases can be considered:

1) In the case when r_1 is at perigee, the true anomaly of $\mathbf{r}_1$ is $\varphi_1 = 0$, then $r_1 = a(1-e)$, and

$$r_2 = \frac{a(1-e^2)}{1 + e\cos\varphi_2} \tag{8}$$

where $\varphi_2 = \theta$ is the true anomaly of $\mathbf{r}_2$. Since $r_1 = a(1-e)$ then

$$\frac{r_2}{r_1} = \frac{1+e}{1+e\cos\theta} \in \left[1, \frac{2}{1+\cos\theta}\right] \tag{9}$$

For those given r_1 and r_2 values not satisfying Eq. (9), P_1 cannot be the perigee.

2) In the case when r_2 is at apogee, the true anomaly of $\mathbf{r}_2$ is $\varphi_2 = \pi$, then $r_2 = a(1+e)$. Following the analysis leading to Eq. (9), the following expression is obtained:

$$\frac{r_1}{r_2} = \frac{1-e}{1+e\cos\varphi_1} = \frac{1-e}{1-e\cos\theta} \in [0, 1] \tag{10}$$

where $\varphi_1 = \pi - \theta$ is the true anomaly of $\mathbf{r}_1$. Equation (10) states that P_2 can be the apogee for any $r_2 \geq r_1$.

Thus, for some values of the perigee distance from the focus $R_p < \min\{r_1, r_2\}$, there may be no orbit satisfying the boundary-value problem, but for any value of the apogee distance from the focus $R_a > \max\{r_1, r_2\}$, there must exist orbits satisfying the boundary-value problem.

V. Eccentricity of Transfer Orbit

The eccentricity of the transfer orbit can be written as [10]

$$e = \sqrt{1 - \frac{4(s-r_1)(s-r_2)}{d^2}\sin^2\left(\frac{\alpha+\beta}{2}\right)} \tag{11}$$

Using Eq. (11) and the definition of angle variables, α and β, the eccentricity becomes a function of only one parameter, the semimajor axis of transfer orbit (see Fig. 4). In addition, the eccentricity of the long-path orbit is greater than that of the short-path orbit for the same semimajor axis and for any transfer angle $0 < \theta < 2\pi$.

Next, the curve characteristics of e are given. Differentiating Eq. (11) with respect to a gives

$$\frac{\mathrm{d}e}{\mathrm{d}a} = \frac{(s-r_1)(s-r_2)\sin(\alpha+\beta)}{ed^2}\frac{1}{a}\left(\tan\frac{\alpha}{2} + \tan\frac{\beta}{2}\right) \tag{12}$$

The minimum is obtained from $\mathrm{d}e/\mathrm{d}a = 0$, which yields

$$\sin(\alpha+\beta) = 0 \to \alpha + \beta = k\pi \tag{13}$$

or

$$\tan\left(\frac{\alpha}{2}\right) + \tan\left(\frac{\beta}{2}\right) = 0 \tag{14}$$

from which the following relationships are obtained:

$$\tan^2\left(\frac{\alpha}{2}\right) = \tan^2\left(\frac{\beta}{2}\right) \to \frac{1-\cos\alpha}{1+\cos\alpha} = \frac{1-\cos\beta}{1+\cos\beta} \tag{15}$$

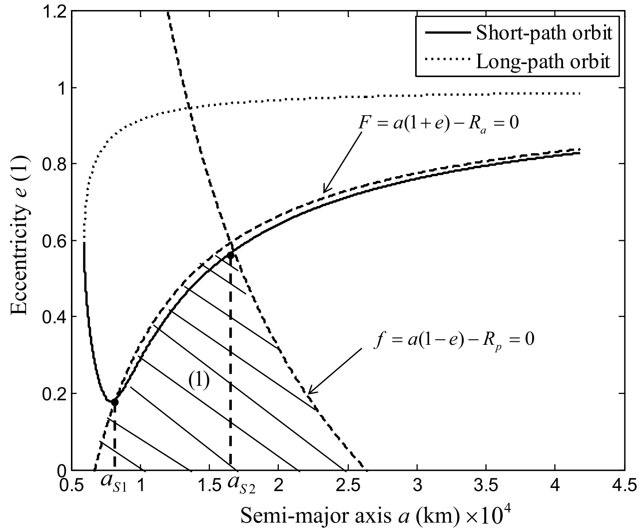

Fig. 4 Eccentricity as provided by Eq. (11) for $r_1 = 7,178.137$ km and $r_2 = 14,356.274$ km.

Multiplying both sides of Eq. (15) by $(1+\cos\alpha)(1+\cos\beta)$, the condition

$$\cos\alpha = \cos\beta \tag{16}$$

is obtained. However, Eq. (3) indicates that there is no solution for Eq. (16). Therefore, Eq. (14) provides no solution for all transfer orbits.

However, solving Eq. (13) shows that $a = (r_1 + r_2)/2$ for the short-path orbit, and there is no solution for the long-path orbit. So for a short-path orbit, there is a single solution for $\mathrm{d}e/\mathrm{d}a = 0$; but for a long-path orbit, there is no solution for $\mathrm{d}e/\mathrm{d}a = 0$. In addition, Eq. (11) indicates that $\lim_{a\to+\infty} e = 1$ for all the transfer orbits, so the solution $a = (r_1 + r_2)/2$ is the minimal value for a short-path orbit.

Finally, an example is given for the $e(a)$ curve. Consider the case with $r_1 = 7,178.137$ km, $r_2 = 14,356.274$ km, and $\theta = \pi/3$, with $R_p = R_E + 350$ km and $R_a = R_E + 20,000$ km as bounds constraints. The curve is plotted in Fig. 4. The figure shows that e is monotonically increasing for a long-path orbit but there is a minimal value for a short-path orbit. The area labeled (1) satisfies the bounds. The range of semimajor axis is $a \in (a_{S1}, a_{S2})$ for a short-path orbit and there is no solution for a long-path orbit.

The constraints on perigee and apogee give the areas of solutions in the figure e vs a, which satisfy the bounds. Then, the range of semimajor axis can be shown distinctly in the figure. In the following sections, the exact value of the semimajor-axis ranges is derived.

VI. Lower Bound on Perigee Altitude

In engineering applications, the perigee altitude is at least greater than a given minimum value. A lower bound can be given as

$$a(1-e) > R_p \tag{17}$$

Then the semimajor-axis range satisfying Eq. (17) is solved. This gives

$$f = a(1-e) - R_p \tag{18}$$

Then inequality (17) becomes $f > 0$. Equation (11) shows that for the same value of a, f of the short-path orbit is greater than that of the long-path orbit. The condition $f > 0$ implies

$$1 - \frac{R_p}{a} > e \tag{19}$$

Using the following trigonometric properties,

$$\sin^2\left(\frac{\alpha+\beta}{2}\right) = \frac{1-\cos(\alpha+\beta)}{2}$$
$$\cos(\alpha+\beta) = \cos\alpha\cos\beta - \sin\alpha\sin\beta \tag{20}$$

then squaring both sides of Eq. (19) gives

$$\left(\frac{R_p}{a}\right)^2 - \frac{2R_p}{a} > -\frac{2(s-r_1)(s-r_2)}{d^2}[1-\cos(\alpha+\beta)] \tag{21}$$

Substituting the value of α and β into Eq. (21) yields

$$\left[\frac{2R_p}{K} + (2s-d)\right]a - \left(\frac{R_p^2}{K} + s(s-d)\right) > \pm\sqrt{s(2a-s)[2a-(s-d)](s-d)} \tag{22}$$

where $K = -2(s-r_1)(s-r_2)/d^2 < 0$. In the above expression, the $-$ sign must be adopted for the short-path orbit and the $+$ sign must be adopted for the long-path orbit. Then let a_1 and a_2 (with $a_1 < a_2$) be two solutions of the following equation:

$$\left[\frac{2R_p}{K} + (2s-d)\right]a - \left(\frac{R_p^2}{K} + s(s-d)\right) = \pm\sqrt{s(2a-s)(s-d)[2a-(s-d)]} \tag{23}$$

Squaring Eq. (23) gives

$$\left[\left(\frac{2R_p}{K}\right)^2 + \frac{4R_p}{K}(2s-d) + d^2\right]a^2 + \left[(4s^3 - 6ds^2 + 2d^2s) - L\left(\frac{4R_p}{K} + 4s - 2d\right)\right]a + \left(\frac{R_p^2}{K}\right)^2 + \frac{2R_p^2}{K}s(s-d) = 0 \tag{24}$$

where $L = R_p^2/K + s(s-d)$. For the above quadratic equation in a, it is easy to get the solutions of a_1 and a_2. Substitute the value of a_1 and a_2 into the left side of Eq. (23) and calculate the values separately. It is a solution for the long-path orbit when the value is positive and for the short-path orbit when the value is negative.

The proof that f monotonically decreases for the long-path orbit is presented. This condition implies

$$\frac{\mathrm{d}f}{\mathrm{d}a} = 1 - e - a\frac{\mathrm{d}e}{\mathrm{d}a} < 0 \tag{25}$$

for all values of a. Multiplying both sides of the above inequality by $(1+e)$ gives

$$1 - e^2 < a(1+e)\frac{\mathrm{d}e}{\mathrm{d}a} \tag{26}$$

Substituting Eqs. (11), (12), and (20) into the above expression and simplifying yields

$$2[1-\cos(\alpha+\beta)] < \sin(\alpha+\beta)\left[\tan\left(\frac{\alpha}{2}\right) + \tan\left(\frac{\beta}{2}\right)\right]\frac{e+1}{e} \tag{27}$$

Because e increases monotonically for a long-path orbit and $e < 1$, inequality (27) is satisfied when

$$1 - \cos(\alpha+\beta) \le \sin(\alpha+\beta)\left(\tan\frac{\alpha}{2} + \tan\frac{\beta}{2}\right) \tag{28}$$

Rewriting inequality (28) gives

$$\begin{aligned} 1-\cos(\alpha+\beta) &\le \sin(\alpha+\beta)\frac{\tan\frac{\alpha}{2} + \tan\frac{\beta}{2}}{1-\tan\frac{\alpha}{2}\tan\frac{\beta}{2}}\left(1-\tan\frac{\alpha}{2}\tan\frac{\beta}{2}\right) \\ &= \sin(\alpha+\beta)\tan\left(\frac{\alpha}{2}+\frac{\beta}{2}\right)\left(1-\tan\frac{\alpha}{2}\tan\frac{\beta}{2}\right) \\ &= [1-\cos(\alpha+\beta)]\left(1-\tan\frac{\alpha}{2}\tan\frac{\beta}{2}\right) \end{aligned} \tag{29}$$

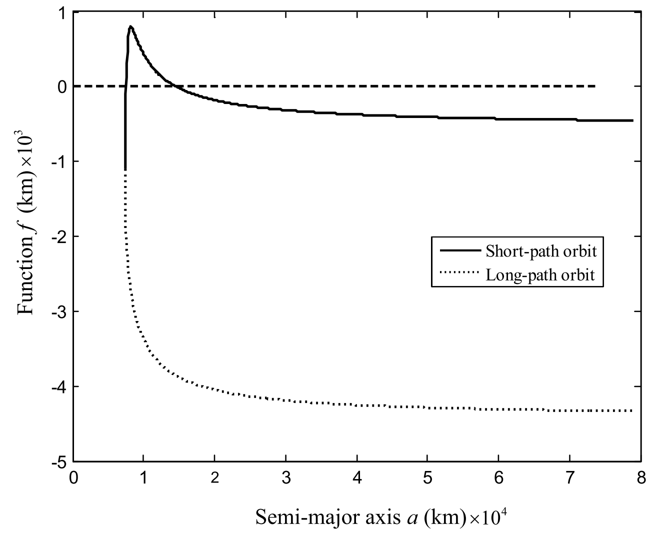

Fig. 5 Case 1a, two solutions for $f = 0$.

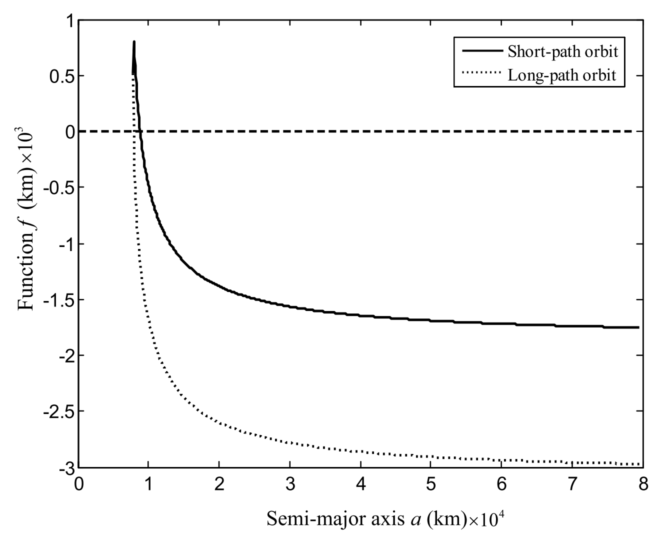

Fig. 6 Case 1b, two solutions for $f = 0$.

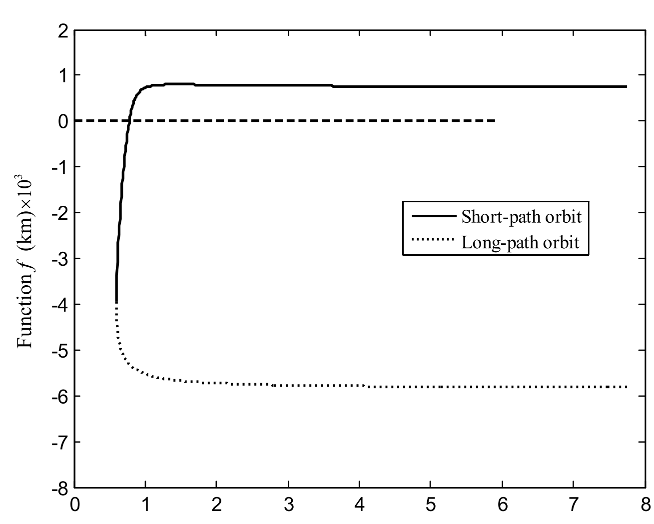

Fig. 7 Case 2a, a single solution for $f = 0$.

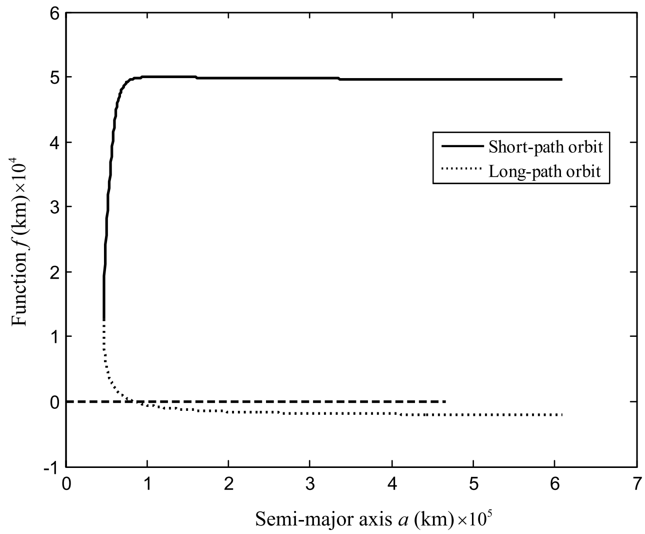

Fig. 8 Case 2b, a single solution for $f = 0$.

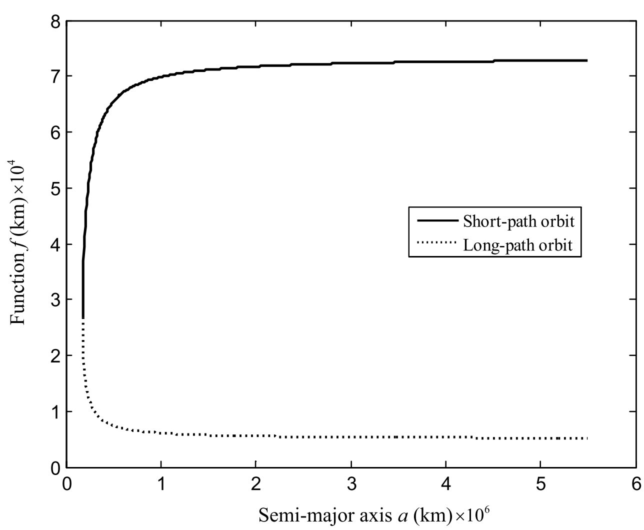

Fig. 9 Case 3a, no solution for $f = 0$.

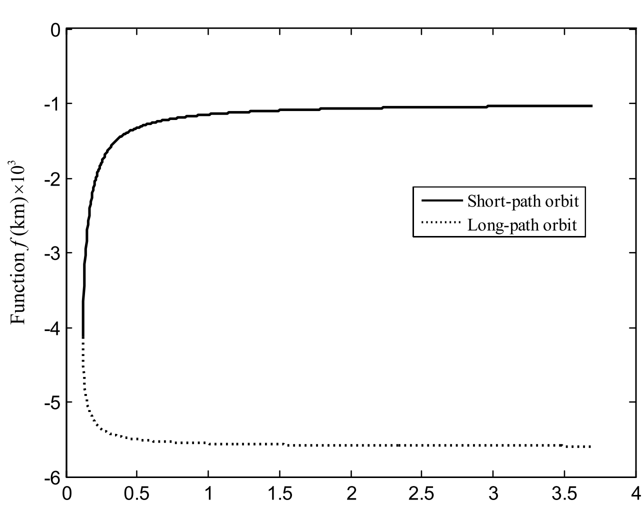

Fig. 10 Case 3b, no solution for $f = 0$.

From the geometric interpretation given in [14] of the variables α and β, the following ranges

$$\frac{\alpha}{2} \in \left[\frac{\pi}{2}, \pi\right] \quad \text{and} \quad \frac{\beta}{2} \in \left[0, \frac{\pi}{2}\right] \quad \text{for } \theta \leq \pi$$
$$\frac{\alpha}{2} \in \left[0, \frac{\pi}{2}\right] \quad \text{and} \quad \frac{\beta}{2} \in \left[-\frac{\pi}{2}, 0\right] \quad \text{for } \theta \geq \pi$$

This implies that for the long-path orbit the following expression,

$$[1 - \tan(\alpha/2)\tan(\beta/2)] \geq 1 \tag{30}$$

is satisfied for all values of a and all values of θ.

Using inequality (30), it can be seen that inequality (29) is satisfied for any long-path orbit. So the curve f decreases monotonically for any long-path orbit with any value of θ. Note that all semimajor axes must satisfy $a > a_m = s/2$ for the transfer orbits, so there are three scenarios to consider.

1) If $a_1 > a_m$, then there are two solutions and two cases:

a) Both of these solutions are for the short-path orbit. In this case (see Fig. 5), the condition $a_1 < a < a_2$ is obtained for a short-path orbit and there is no solution for a long-path orbit.

b) One solution is for a short-path orbit and the other is for a long-path orbit. This is shown in Fig. 6, where $a_m \leq a < a_2$ is obtained for a short-path orbit and $a_m \leq a < a_1$ is obtained for a long-path orbit.

2) If $a_1 \leq a_m \leq a_2$, then there is a single solution and two cases:

a) A single solution is obtained for a short-path orbit. In this case (see Fig. 7) $a > a_2$ is obtained for a short-path orbit and there is no solution for a long-path orbit.

b) A single solution is obtained for a long-path orbit. This is shown in Fig. 8, where $a_m \leq a < a_2$ is obtained for a long-path orbit and all the conditions $a \geq a_m$ are obtained for a short-path orbit.

3) If $a_m > a_2$, then there is no solution and two cases:

a) $f > 0$ for all the $a \geq a_m$ (see Fig. 9);

b) $f < 0$ for all the $a \geq a_m$ (see Fig. 10).

Finally, the limit of f (for $a \to +\infty$) can be obtained as it follows:

$$\begin{aligned}
\lim_{a\to+\infty} f &= \lim_{a\to+\infty} a\frac{1-e^2}{1+e} - R_p \\
&= \lim_{a\to+\infty}\left(\frac{(s-r_1)(s-r_2)}{d^2}a[1-\cos(\alpha+\beta)]\right) - R_p \\
&= -R_p + \frac{(s-r_1)(s-r_2)}{d^2}\lim_{a\to+\infty}\left(a\left[1-\left(1-\frac{s}{a}\right)\left(1-\frac{s-d}{a}\right)\right.\right. \\
&\quad \left.\left.\pm\sqrt{\frac{s}{a}\left(2-\frac{s}{a}\right)\frac{s-d}{a}\left(2-\frac{s-d}{a}\right)}\right]\right) \\
&= -R_p + \frac{(s-r_1)(s-r_2)}{d^2}(2s-d\pm 2\sqrt{s(s-d)})
\end{aligned} \tag{31}$$

In Eq. (31), the $+$ sign must be adopted for a short-path orbit and the $-$ sign must be adopted for a long-path orbit.

VII. Upper Bound on Apogee Altitude

In addition to a lower bound on the perigee altitude, there is usually an upper bound on the apogee altitude. Suppose a constraint on the apogee is expressed as

$$a(1+e) < R_a \tag{32}$$

Letting

$$F = a(1+e) - R_a \tag{33}$$

then inequality (32) becomes $F < 0$. Equation (11) indicates that the F of the long-path orbit is greater than that of the short-path orbit for any value of a. The derivative of F with respect to a is

$$\frac{dF}{da} = 1 + e + a\frac{de}{da} \tag{34}$$

Using the relationship between e and a and Eq. (12), the condition $dF/da > 0$ is obtained for any a of long-path orbits, but for short-path orbits, the value of dF/da is negative infinity for all values of θ when $a \to a_m^+$. The differential value of F is equal to 2 (positive) for all values of θ when $a \to +\infty$, so there exists a semimajor axis satisfying $dF/da = 0$.

In addition, the equation $F = 0$ gives an analogous quadratic equation to Eq. (24) by only replacing R_p with R_a. So there are two solutions in total (a_3 and a_4, with $a_3 \le a_4$). For any $R_a \ge \max\{r_1, r_2\}$, there are two cases:

1) There are two solutions for $F = 0$: a_3 is for a long-path orbit, and a_4 is for a short-path orbit (see Fig. 11). In this case, the range is $a_m \le a < a_3$ for a long-path orbit and $a_m \le a < a_4$ for a short-path orbit.

2) There are two solutions for $F = 0$: both are for a short-path orbit, so the range is $a_3 < a < a_4$ for a short-path orbit and there is no solution for a long-path orbit (see Fig. 12).

Remark: For assigned values of r_1, r_2, and θ, solving the $f > 0$ constraint gives a range of a, while solving the $F < 0$ constraint gives a different range of a. Then the intersection range of the above two ranges (which are $a_{S1} < a < a_{S2}$ for the short-path orbit and $a_{L1} < a < a_{L2}$ for the long-path orbit, where a_{S1} and a_{L1} may be a_m or no solution, and a_{S2} and a_{L2} may be positive infinity or no solution) can be computed.

With the intersection range of a for fixed transfer time t_f, the allowed number of revolutions is solved and then all the feasible solutions of a are calculated.

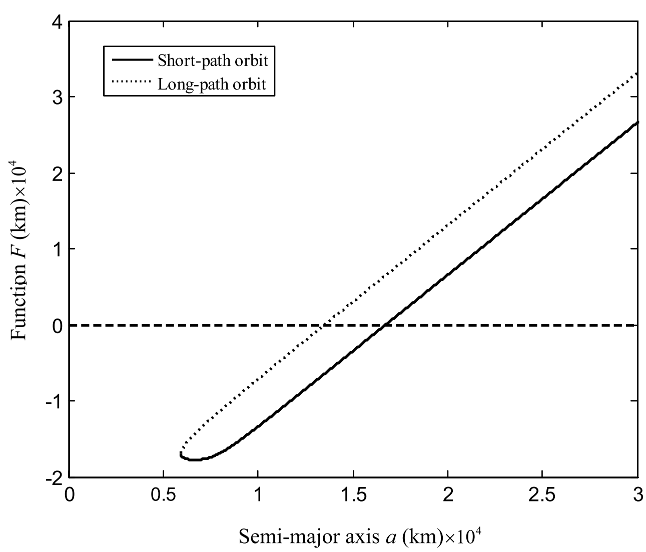

Fig. 11 Case 1, two solutions for $F = 0$.

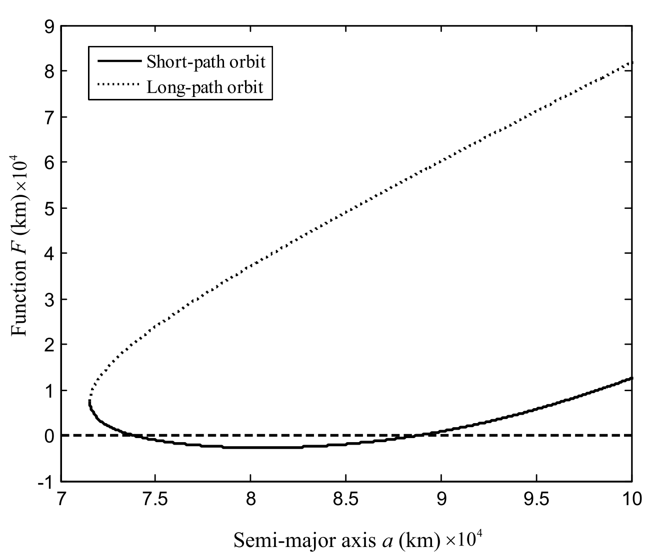

Fig. 12 Case 2, two solutions for $F = 0$.

VIII. Solving for the Semimajor Axis for Each Feasible Orbit

Lagrange's transfer time given in Eq. (2) can be rewritten as

$$N(a) = \frac{1}{2\pi}[\sqrt{\mu}t_f a^{-3/2} - (\alpha - \beta - \sin\alpha + \sin\beta)] \tag{35}$$

For a fixed transfer time t_f, the allowed number of revolutions N is only a function of the semimajor axis. Performing the derivative of Eq. (35), the following expression is obtained:

$$\frac{dN}{da} = \frac{1}{2\pi}\left[-\frac{3}{2}\sqrt{\mu}t_f a^{-5/2} + \frac{1}{a}\left(\tan\frac{\alpha}{2} - \tan\frac{\beta}{2} - \cos\alpha\tan\frac{\alpha}{2} + \cos\beta\tan\frac{\beta}{2}\right)\right] \tag{36}$$

From $dN/da = 0$, the solution $a_{\max}$ can be obtained. Note that $a_{\max}$ is a solution of the lower branch in the curve of t_f vs a, so N is monotonically decreasing for the upper branch (see Fig. 13). When $a = a_{\max}$ for the lower branch, the maximum number of revolutions is given by

$$N_{\max} = \lfloor N(a_{\max}) \rfloor \tag{37}$$

where the function $\lfloor y \rfloor$ denotes the nearest integer less than or equal to y. This is another method to solve for $N_{\max}$ apart from inequality (5).

Next, the allowed number of revolutions is solved for Lambert's problem with bounds. Assume that $\theta \le \pi$, which implies no loss of generality. The lower branch denotes the short-path orbit. In this case, N is monotonically decreasing for a long-path orbit and there is a solution $a_{\max}$ of $dN/da = 0$ for a short-path orbit. Assume that the solved ranges of semimajor axis are $a_{S1} < a < a_{S2}$ for a short-path orbit and $a_{L1} < a < a_{L2}$ for a long-path orbit. For the long-path orbit, the range of N is

$$\lceil N(a_{L2}) \rceil \le N \le \lfloor N(a_{L1}) \rfloor, \qquad N \in Z^+ \tag{38}$$

where the function $\lceil y \rceil$ denotes the nearest integer greater than or equal to y, and Z^+ is the set of positive integers. For the short-path orbit, there are three cases:

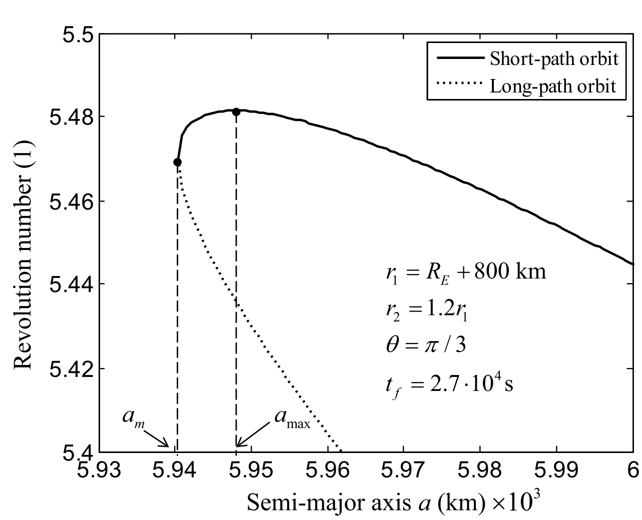

Fig. 13 Revolution number.

1) If $a_{S1} > a_{\max}$, then $\lceil N(a_{S2}) \rceil \le N \le \lfloor N(a_{S1}) \rfloor$ ($N \in Z^+$).
2) If $a_{S2} < a_{\max}$, then $\lceil N(a_{S1}) \rceil \le N \le \lfloor N(a_{S2}) \rfloor$ ($N \in Z^+$).
3) If $a_{S1} \le a_{\max} \le a_{S2}$, then $\lceil \min\{N(a_{S1}), N(a_{S2})\} \rceil \le N \le \lfloor N(a_{\max}) \rfloor$ ($N \in Z^+$).

Based on the allowed number of revolutions, the solutions of the semimajor axis can be obtained by Eq. (2) for each possible orbit. Note that when inequality (6) is satisfied for $N = N_{\max}$, there are two solutions for a short-path orbit. One solution may not be included in the range of (a_{S1}, a_{S2}), so in this case, it must be deleted from the possible solution space.

IX. Discussion of $N = 0$

Previously, a lower bound on the perigee altitude and an upper bound on the apogee altitude have been analyzed. But when $N = 0$, the trajectory may not pass through the perigee or the apogee and, as such, it should be discussed separately. Define the magnitude of radius vector as $r_i = (1 - e^2)/(1 + e\cos\varphi_i)$, $i = 1, 2$, and φ_i as the true anomaly. Let $\varphi_{10} = \cos^{-1}[(1 - e^2)/(er_1) - 1/e]$ and $\varphi_{20} = \cos^{-1}[(1 - e^2)/(er_2) - 1/e]$. Note that $\varphi_{10} \in [0, \pi]$, $\varphi_{20} \in [0, \pi]$, so the true anomalies φ_1, φ_2 can be obtained as follows:

1) If $\varphi_{20} - \varphi_{10} = \theta$ or $2\pi + \varphi_{20} - \varphi_{10} = \theta$, then $\varphi_1 = \varphi_{10}$ and $\varphi_2 = \varphi_{20}$.
2) If $2\pi - \varphi_{20} - \varphi_{10} = \theta$, then $\varphi_1 = \varphi_{10}$ and $\varphi_2 = 2\pi - \varphi_{20}$.
3) If $\varphi_{20} + \varphi_{10} = \theta$, then $\varphi_1 = 2\pi - \varphi_{10}$ and $\varphi_2 = \varphi_{20}$.
4) If $-\varphi_{20} + \varphi_{10} = \theta$ or $2\pi - \varphi_{20} + \varphi_{10} = \theta$, then $\varphi_1 = 2\pi - \varphi_{10}$ and $\varphi_2 = 2\pi - \varphi_{20}$.

From the values of φ_1 and φ_2 the passage through the perigee or the apogee can be verified. If it only passes through the perigee, then only the lower bound has to be considered. If it only passes through the apogee, then only the upper bound has to be considered. If it passes through both perigee and apogee, then both lower and upper bounds as previously derived must be considered. Note that for $N = 0$, the proposed method indeed eliminates the unfeasible branches after solving Lambert's problem.

X. Numerical Example

Assume the initial magnitude of radius vector $r_1 = R_E + 800$ km, the terminal magnitude of radius vector $r_2 = 1.2r_1$, and transfer angle $\theta = \pi/3$. Figure 3 gives the curve of transfer time as a function of semimajor axis. For the fixed transfer time $t_f = 2.7 \times 10^4$ s, there are 11 possible solutions of the semimajor axis a.

Consider now bounds on both perigee and apogee. Consider the case with $R_p = R_E + 350$ km and $R_a = R_E + 20,000$ km. Figure 7 shows the behavior of $f(a)$. From Eq. (24) and $f > 0$ the condition $a > 8,273.5$ km is obtained for a short-path orbit and there is no solution for a long-path orbit. The figure F vs a is plotted in Fig. 11. From Eq. (24) and $F < 0$ the condition $a_m \le a < 16,777$ km is obtained for a short-path orbit and $a_m \le a < 13,553$ km for a long-path orbit. The final range is $8,273.5 \text{ km} < a < 16,777$ km for a short-path orbit and no solution exists for a long-path orbit. Substituting the range found for a into Eq. (38) and the short-path orbit analysis gives the range of N as $\lceil 1.2065 \rceil \le N \le \lfloor 3.4524 \rfloor$ ($N \in Z^+$) for a short-path orbit, so the final allowed numbers of revolutions are 2 and 3.

When the revolution number is $N = 0$, then the elements of transfer orbit are $a = 20,052$ km for a long-path orbit, $e = 0.9678$, and the true anomalies, $\varphi_1 = 148.25$ deg and $\varphi_2 = 208.25$ deg. This means that it only passes through the apogee. Therefore, only the upper bound must be considered. The above analysis indicates that $a = 20,052$ km is not a solution for $F < 0$ and, consequently, it is not a solution for Lambert's problem with bounds.

From Fig. 14 it is easily seen that there are only two solutions (with large stars) for the multiple-revolution Lambert's problem considering bounds. Both of these solutions are for the short-path orbit. The maximum number of revolutions is 3; the minimum number of revolutions is 2. When $N = 2$, the semimajor axis $a = 11,956$ km; when $N = 3$, the solution $a = 9,099.4$ km.

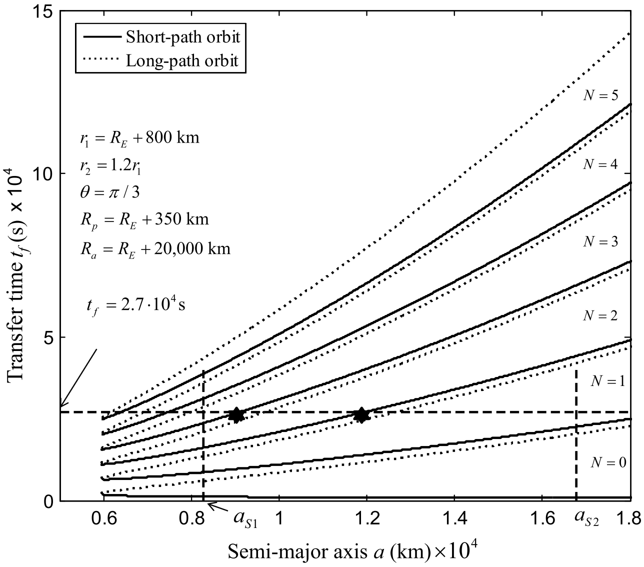

Fig. 14 Plot of t_f vs a with bounds.

XI. Conclusions

In this paper a method for solving the multiple-revolution Lambert's problem with a lower bound on the perigee altitude and an upper bound on the apogee altitude is proposed and numerically tested. First, some characteristics (relationships and inequalities) for short-path orbits and long-path orbits are analyzed and proved. Based on these properties, the range of semimajor axes satisfying the constraints is solved. The case of zero revolutions is separately analyzed, as in this case, the transfer trajectory may not pass through the perigee or apogee. An example is given showing that there might be a substantial reduction of the number of solutions for the transfer orbit when bounds are considered. For this reason, in order to deal with just the feasible solutions, the proposed method finds several applications in aerospace engineering optimization problems. The multiple-revolution orbit determination problems, the n-impulsive orbit transfer and rendezvous problems, as well as transfer trajectory optimization problems are all typical problems in which the proposed method can be implemented.

Acknowledgment

The authors would like to thank Troy Henderson for generously reviewing this manuscript for consistency and formalism.

References

[1] Battin, R. H., *An Introduction to the Mathematics and Methods of Astrodynamics*, Revised ed., AIAA Education Series, AIAA, Reston, VA, 1999, pp. 515–566.
[2] Lagrange J. L., "Sur le Problème de la Determination des Orbites des Comètes d'Après Trois Observations," Memoires 1 and 2, *Nouveaux Mémoires de l'Académie de Berlin*, 1778.
[3] Gauss, K. F., *Theoria Motus Corporum Coelestium in Sectionibus Conicis Solem Ambientium*, edited by F. Perthes and I. H. Besser, 1809; also "Theory of the Motion of the Heavenly Bodies Moving About the Sun," Little, Brown and Co., Boston, 1857 (in English).
[4] Sconzo, P., "The Use of Lambert's Theorem in Orbit Determination," *Astronomical Journal*, Vol. 67, No. 1, Feb. 1962, pp. 19–21. doi:10.1086/108599
[5] Lancaster, E. R., Blanchard, R. C., and Devaneyj, R. A., "A Note on Lambert's Theorem," *Journal of Spacecraft and Rockets*, Vol. 3, No. 9, Sept. 1966, pp. 1436–1438. doi:10.2514/3.28673
[6] Battin, R. H., "Lambert's Problem Revisited," *AIAA Journal*, Vol. 15, No. 5, May 1977, pp. 707–713. doi:10.2514/3.60680
[7] Battin, R. H., and Vaughan, R. M., "An Elegant Lambert Algorithm," *Journal of Guidance, Control, and Dynamics*, Vol. 7, No. 6, 1984, pp. 662–670.

doi:10.2514/3.19910

[8] Gooding, R. H., "A Procedure for the Solution of Lambert's Orbital Boundary-Value," *Celestial Mechanics and Dynamical Astronomy*, Vol. 48, 1990, pp. 145–165.
doi:10.1007/BF00049511

[9] Avanzini, G., "A Simple Lambert Algorithm," *Journal of Guidance, Control, and Dynamics*, Vol. 31, No. 6, 2008, pp. 1587–1594.
doi:10.2514/1.36426

[10] Prussing, J. E., "A Class of Optimal Two-Impulse Rendezvous Using Multiple-Revolution Lambert Solutions," *Advances in the Astronautical Sciences*, Vol. 106, Univelt, San Diego, CA, 2000, pp. 17–39.

[11] Shen, H., and Tsiotras, P., "Optimal Two-Impulse Rendezvous Using Multiple-Revolution Lambert Solutions," *Journal of Guidance, Control, and Dynamics*, Vol. 26, No. 1, 2003, pp. 50–61.
doi:10.2514/2.5014

[12] Luo, Y. Z., Tang, G. J., Lei, Y. J., and Li, H. Y., "Optimization of Multiple-Impulse Multiple-Revolution Rendezvous Phasing Maneuvers," *Journal of Guidance, Control, and Dynamics*, Vol. 30, No. 4, 2007, pp. 946–952.
doi:10.2514/1.25620

[13] He, Q., Li, J., and Han, C., "Multiple-Revolution Solutions of the Transverse-Eccentricity-Based Lambert Problem," *Journal of Guidance, Control, and Dynamics*, Vol. 33, No. 1, 2010, pp. 265–268.
doi:10.2514/1.45041

[14] Prussing, J. E., "Geometrical Interpretation of the Angles α and β in Lambert's Problem," *Journal of Guidance, Control, and Dynamics*, Vol. 2, No. 5, 1979, pp. 442–443.
doi:10.2514/3.55905